Physica Medica 105 (2023) 102512

Contents lists available at ScienceDirect

Physica Medica

journal homepage: www.elsevier.com/locate/ejmp

Realistic 3D printed CT imaging tumor phantoms for validation of image processing algorithms

Sepideh Hatamikia [a,b,c,*], Ingo Gulyas [d], Wolfgang Birkfellner [c], Gernot Kronreif [a], Alexander Unger [a], Gunpreet Oberoi [c], Andrea Lorenz [a], Ewald Unger [c], Joachim Kettenbach [e], Michael Figl [c], Janina Patsch [f], Andreas Strassl [f], Dietmar Georg [d], Andreas Renner [d]

[a] Austrian Center for Medical Innovation and Technology, Wiener Neustadt, Austria
[b] Research Center for Medical Image Analysis and Artificial Intelligence (MIAAI), Department of Medicine, Danube Private University, Krems, Austria
[c] Center for Medical Physics and Biomedical Engineering, Medical University of Vienna, Vienna, Austria
[d] Department of Radiation Oncology, Medical University of Vienna, Vienna, Austria
[e] Institute of Diagnostic, Interventional Radiology and Nuclear Medicine, Landesklinikum Wiener Neustadt, Wiener Neustadt, Austria
[f] Department of Radiology and Nuclear Medicine, Medical University Vienna, Austria

ARTICLE INFO

Keywords:
Medical imaging
3D printing
Realistic tumor phantoms
CT imaging

ABSTRACT

Medical imaging phantoms are widely used for validation and verification of imaging systems and algorithms in surgical guidance and radiation oncology procedures. Especially, for the performance evaluation of new algorithms in the field of medical imaging, manufactured phantoms need to replicate specific properties of the human body, e.g., tissue morphology and radiological properties. Additive manufacturing (AM) technology provides an inexpensive opportunity for accurate anatomical replication with customization capabilities. In this study, we proposed a simple and cheap protocol using Fused Deposition Modeling (FDM) technology to manufacture realistic tumor phantoms based on the filament 3D printing technology. Tumor phantoms with both homogenous and heterogeneous radiodensity were fabricated. The radiodensity similarity between the printed tumor models and real tumor data from CT images of lung cancer patients was evaluated. Additionally, it was investigated whether a heterogeneity in the 3D printed tumor phantoms as observed in the tumor patient data had an influence on the validation of image registration algorithms.

A radiodensity range between −217 to 226 HUs was achieved for 3D printed phantoms using different filament materials; this range of radiation attenuation is also observed in the human lung tumor tissue. The resulted HU range could serve as a lookup-table for researchers and phantom manufactures to create realistic CT tumor phantoms with the desired range of radiodensities. The 3D printed tumor phantoms also precisely replicated real lung tumor patient data regarding morphology and could also include life-like heterogeneity of the radiodensity inside the tumor models. An influence of the heterogeneity on accuracy and robustness of the image registration algorithms was not found.

1. Introduction

Medical imaging offers a wide variety of imaging modalities to gain information required for diagnosis or therapy control. New imaging algorithms need extensive testing and validation. However, the ground truth for validation of different imaging algorithm is hard to obtain. Thus, sophisticated phantom studies are required in order to precisely evaluate the performance of newly developed algorithms. For CT imaging besides realistic morphology, the radiological properties also need to be simulated accurately. The availability of additive manufacturing (AM) technology, colloquially called 3-dimensional (3D) printing, has paved the way towards creation of realistic models and imaging phantoms for specific research purposes in many fields as well as in radiation therapy (RT) [1–5,6,7]. CT-derived 3D printed anatomical models allow for creating patient-equivalent structures with lifelike shape and internal structure [1,5]. So far, several phantoms have been developed to mimic bone and soft tissue related to different site in the body [8–11]. In addition, computational tumor models which are mathematical

* Corresponding author at: Viktor Kaplan-Straße 2/1, 2700 Wiener Neustadt, Austria.
E-mail address: sepideh.hatamikia@acmit.at (S. Hatamikia).

https://doi.org/10.1016/j.ejmp.2022.102512
Received 18 June 2022; Received in revised form 6 November 2022; Accepted 15 December 2022
Available online 28 December 2022

computer-based breast lesion models with realistic shape have been proposed [12,13]. However, the possibility of fabricating sophisticated phantoms that mimic both, the X-ray attenuation properties and the morphology of the patient's tumor tissue, has not yet been extensively investigated. Realistic tumor phantoms are required for validation of different image processing algorithms such as registration algorithms (e.g., tumor tracking for tumor motion monitoring in RT) and image segmentation (e.g., validation of advanced automatic segmentation methods). Based on our knowledge, there is no study describing a methodology suitable to manufacture realistic tumors with both human-like morphology and radiodensity suitable for CT imaging. In addition, the influence of tumor-like heterogeneous radiodensity distributions in imaging phantoms was not investigated in the previous literature. Thus, the question whether a simplification introduced by the imaging phantom (e.g homogenous radiodensity other than heterogenous) in a validation study affects the accuracy of the developed imaging algorithm could not be answered.

An important aspect in the development of a suitable radiological phantom is the use of appropriate printing materials [14]. Some studies have tried to replicate realistic radiation attenuation properties for tumor phantoms using different 3D printer-based technologies and materials. In a study [15], a life-size thorax phantom including different tumors was developed using 3D printing technology based on a clinical CT scan from a lung cancer patient in order to closely resemble patient structure and tissue radiodensity. Three lung tumors were printed using nylon material based on Selective Laser Sintering (SLS) technique. Although their 3D printed results showed a comparable result with patient CT regarding the shape, size and structure, the Hounsfield units (HU) were not similar to those of the patient CT data. In another study [16], authors used Acrylonitrile Butadiene Styrene (ABS)-M30 thermoplastic material to print a tumor replica based on a non-small cell lung cancer (NSCLC) patient CT data. Their 3D printed tumor was used to investigate dosimetric experiments and imaging purposes using an advanced breathing phantom (ARDOS). Although authors claimed that their tumor phantom provided a realistic shape and HU parameters, they did not report the radiodensity value of the manufacture's tumor phantom and its correspondence to the real patient data. In another study [17], agar-gelatin-based tumor phantoms were developed which could both visually and radiographically mimic typical head and neck squamous cell carcinoma (HNSCC). Tumor phantoms were used in a cadaver model and a radiodensity between 59 and 127 HU (mean 93.7) was achieved which was in a good agreement with the patient tumor radiodensity. However, the inserted tumor could not mimic a realistic tumor shape. In addition, their proposed tumor phantom does not mimic the radiodensity heterogeneity that is seen with most HNSCC [17]. In a recent study [18], authors proposed two types of approaches to fabricate lung tumor phantoms including 3D-printed tumor phantoms using glycol-modified polyethylene terephthalate (PET-G) and also using sodium polyacrylate plus iodinated contrast medium. The goal was to construct heterogeneous inserts mimicking a target tissue for robustness analysis in radiomic studies. In another study [19], the authors proposed manufacturing realistic patient-derived breast phantoms with different tissues using polylactic acid (PLA) filament. An HU of 64 was selected for the creation of the breast tumor phantom. 3D printed compressed breast phantoms were also developed using acrylonitrile–butadiene–styrene (ABS), PLA and PET filaments (100 % infill density) for replicating adipose tissue, glandular and skin tissues, respectively for digital mammography (DM) and digital breast tomosynthesis (DBT) X-ray imaging [20]. In this study, we propose a simple protocol for manufacturing human-like imaging tumor phantoms regarding morphology and radiodensity using filament printing technology. Different filament materials were investigated in order to find their correspondence with realistic radiodensity range in patient tumor data and a radiodensity spectrum with a good match to the lung patient tumor radiodensity range was explored. In addition, a look-up table with a HU range between −217 and 226 was introduced to serve as a recipe for researchers to create their individual customized CT tumor phantoms (for different types of tumors) with the desired range of radiodensities. As an additional analysis, 3D-printed realistic tumor phantoms capable of simulating the heterogeneous structure and radiological characteristics of tumors found in CT of lung cancer patients were studied and the effects of using heterogeneous tumor phantom compared to a homogeneous tumor phantom on the performance of the image registration algorithms were evaluated.

2. Materials and methods

2.1. Patient data

In this study, we investigated the CT data from seventeen lung cancer patients. The data used in this study was approved by the Ethics Committee of the Medical University of Vienna (EK1253/2012). Anonymized patient CT data (SOMATOM Definition AS, Siemens Healthineers, Germany, tube voltage 120 kVp, tube current time product 315 mAs) including Digital Imaging and Communication in Medicine (DICOM) data files was used.

2.1.1. Determination of realistic HU range in patient tumor CT data

The CT from different patient tumor data showed large differences in the shape and size. Five examples of the patient tumor data with different sizes are shown in Fig. 1a. We evaluated the radiation attenuation property of the tumors by determining HU values corresponding to the segmented CT data. A HU spectrum analysis was performed in order to quantify the HU distribution of the tumor voxels. Furthermore, in order to investigate HU inhomogeneity (or distribution) within the tumor, the Segmentations module from 3D Slicer software 4.10.2 (Salt Lake City, Utah, USA) was used to segment the tumor according to different HU ranges for identifying regions with specific HU ranges. The HU analysis (Section 2.7) using all patient tumors demonstrated a HU range between −100 to 100 for most of patient tumors. In addition, a higher radiodensity (an average range between 0 and 100 HU ($=50 \pm 34$)) in the centroid of the tumor while lower radiodensity (an average range between −100 to 0 HU ($=-50 \pm 29$)) in the outer areas of the tumor was observed which showed a HU heterogeneity within different areas inside the tumor. Visualization of a HU spectrum and the corresponding tumor segmented regions for one example of patient data is illustrated in Fig. 1b–f.

2.2. 3D phantom design

SlicerRT module in 3D Slicer was used for designing the tumor phantoms. The segmentation of the clinical target volume (CTV) was used to extract the tumor volume from the CT patient data in order to create the tumor models. The tumor segmentation was exported as STL (Standard Tessellation Language) file to extract the smoothed tumor surface used as input data for the PrusaSlicer Software 2.3.0 (Prusa Research a.s., Praha, Czech Republic) for the 3D printing procedure. For the heterogenous tumor models, two separate models were created from the segmented inner and outer areas of the tumors (e.g. segmented areas as shown in Fig. 1b–d). In this study, two different tumor models with different tumor volume were used: tumor model 1 originating from the patient 1 CT data and tumor model 2 originating from the patient 4 CT data (Fig. 1a). A 3D visualization of designed tumor models after rendering in Autodesk Meshmixer software 3.5.474 (Portland, Oregon, USA) software is shown in Fig. 2A

2.3. Additive manufacturing using filament printing technology

Using Fused Deposition Modeling (FDM) technology, a 3D object is printed layer by layer by extruding a filament through a nozzle. The filament can be printed in a wide variety of grid patterns, which is called infill, and the infill density (material:air ratio) can be set in %. Using this

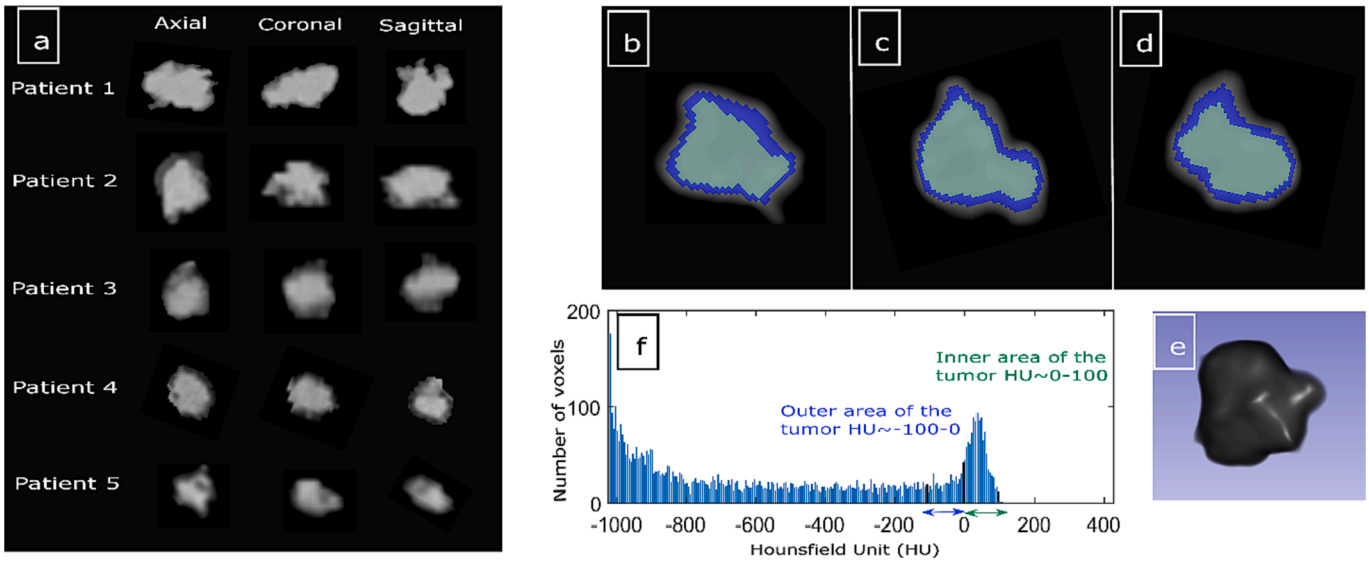

Fig. 1. (a) Five examples of the patient tumor CT data with different sizes, CT segmentation of one sample tumor (patient 4) in three different views (b–d) as well as 3D representation in 3D Slicer (e) and the corresponding HU spectrum (f) in order to visualize the HU inhomogeneity within the tumor. The spectrum in the range of −1000 to −200 HU is related to surrounding lung tissue.

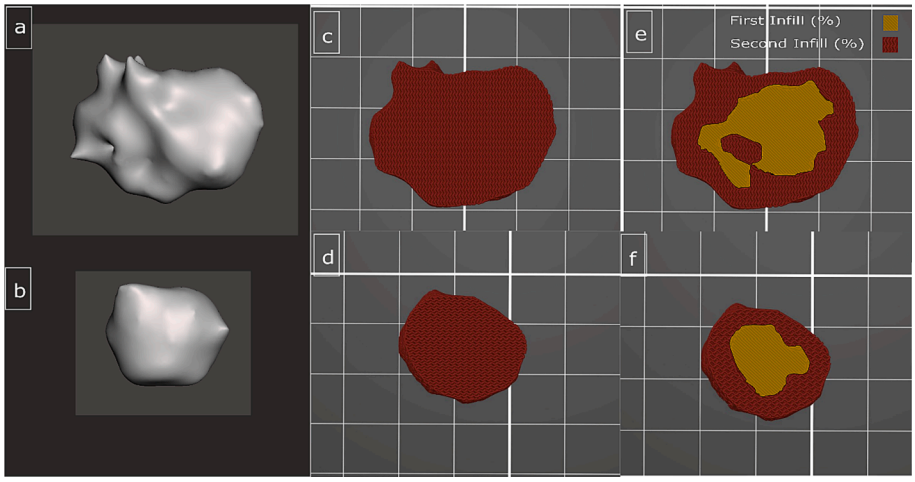

Fig. 2. (a, b) 3D visualization of the tumor models in Autodesk Meshmixer software. Illustration of the design of the homogenous (c, d) and heterogenous (e, f) for both tumor models in the PrusaSlicer software. Difference between infill densities used for the inner area and outer areas of hetrogenous tumor is visible (e, f).

technique, prints even with the highest infill density might include air gaps in the sub-millimeter scale. This feature makes this technique suitable to manufacture realistic imaging phantoms, which are able to simulate a grey value spectrum equivalent to the radiation attenuation of human tissues by means of varying the infill density parameter.

In a study [21], the radiological properties of a variety of 3D printing materials were evaluated for different ranges of photon energies. Using FDM printer, the ABS and PLA filaments were printed with variety of infill densities to achieve different CT values approximating the CT values of low-density lung, high-density lung and soft tissues. In another study [22], authors also investigated a large set of commercially available 3D-printed samples from different plastic materials to evaluate their radiological properties. The main focus was to find suitable tissue-equivalent 3D-printed plastics materials for medical phantoms which are used in radiology. In this study, we investigated different FDM-based filament materials and finally introduced the most promising materials with suitability for mimicking lung tumor radiation attenuation properties as observed in lung cancer patient datasets.

2.4. Creation of cylindric samples with specific radiation attenuation properties

In order to determine the infill densities that reproduce different radiodensities comparable with the patient tumor CT we evaluated a large set of different filament materials and varied the infill density parameter of the print. A cylinder model with the diameter of 2 cm and length of 7 cm was designed for the test printing. For each filament material, a set of 7 infill densities including 100 %, 97 %, 94 %, 91 %, 88 %, 85 %, 82 % (called as Infill 1, Infill 2, … Infill 7) was used to reproduce a gradient in HU range within a cylinder. Four different filament materials including Polylactic acid (PLA), Polayamid 12 (Nylon12 or PA12), Acrylonitrile styrene acrylate (ASA Pro), Polyethylenterephthalat (PETG) were selected and reported in this study due to their similarity to the patient tumor radiodensity range. In addition, a set of 22 infill densities including 100 % to 79 % with infill step size of 1 % was used for two additional cylinders (PLA and PETG) with similar cylinder size as before. This experiment was done to investigate whether a continuous change of the HU can be achieved within the printed

model.

2.5. Radiodensity values selected to be replicated in the tumor phantom

For each of the two tumor models originating from patient 1 and patient 4 (Section 2.2), three heterogenous and three homogenous samples with different infill densities were designed (12 tumor samples in total). The selection of infill densities for the samples was done after matching the resulted HU values achieved from the cylinders CT with the corresponding CT values in the patient tumor scans. Different infill densities were used for different tumor samples in order to simulate different HU range as observed in the patient dataset (Table 1). In addition, the density of all 3D printed phantoms was calculated by dividing the weight (g) of each printed tumor to the volume (cm3) of the tumor (calculated from the CT of each tumor phantom). The density of ASA, PLA, Nylon and PETG are reported as 1.08 (g/cm3), 1.29 (g/cm3), 1.18 (g/cm3) and1.30 (g/cm3), respectively [23,24].

2.6. Additive manufacturing of the tumor phantoms

The 3D printing was done using a custom filament 3D printer (Original Prusa i3 MK3S, Prusa Research a.s., Praha, Czech Republic). The G-Code for printing was prepared with the PrusaSlicer Software. A Gyroid pattern was used for the infill. Infill density was adapted to match the respective HU values. The layer resolution was set to 0.2 mm for all samples. Printing temperature and speeds were selected based on the filament manufacturer and 3D printer specifications. In order to define different infill densities for inner and outer areas for heterogenous tumors in PrusaSlicer (Fig. 2 e, f), the whole STL model was imported as one part and different sub-parts were added as modifiers. 12 tumor phantoms were printed according the 12 tumor samples designed as described in Section 2.5.

2.7. HU analysis of the patient CT, tumor phantom and test samples

The test printed cylinders as well as the 12 tumor phantoms were scanned in a CT (Section 2.1) with the standard clinical CT protocol (tube current time product 315 mAs, tube voltage 120 kVp, slice thickness 2 mm, pixel spacing 0.68 mm) in order to evaluate their radiodensity properties. We used the Analyze 12.0 toolkit (AnalyzeDirect, Overland Park, United States) in order to measure the HU values from the CT scan related to patients, printed cylinders and printed tumor phantom. The HU analysis was done by selecting different line profiles inside the corresponding region and measuring the HU by calculating the average and the standard deviation over all points for the selections related to those line profiles.

2.8. Physical dimensional comparison between the phantom and patient STL

The FDM printed tumor samples were individually scanned using a high-resolution photon-counting CT scanner (NAEOTOM Alpha, VA40A, Siemens Healthineers, Forchheim, Germany, tube current time product 200 mAs, tube voltage 120 kVp, slice thickness 0.2 mm, pixel spacing 0.09 mm) in order to evaluate their geometry accuracy as compared to the original tumor model. The resulted DICOM files were exported to the segmentation and modelling software Materialize Mimics Research 23.0 (Materialize, Leuven, Belgium) for a semi-automatic thresholding of the tumor samples. All samples were segmented and exported to the designing software Materialize 3-Matic 15.0 for dimensional comparison (Fig. 3). The software gave volume and surface area information of the samples and patient tumor models (Table 2). Both manual alignments followed by automatic *N*-point registration of the printed tumor models over the patient tumor models was performed by a single operator, and overlapping volume was calculated manually and as well as using Collision detection analysis, for each sample. The latter detects intersections that occur between multiple parts and calculates the colliding volume.

Table 1
Infill densities and materials used for all samples for tumor models 1 and 2.

	Sample 1	Sample 2	Sample 3
Homogenous tumor model 1	Material: PLA Total area: Infill 7	Material: PLA Total area: Infill 3	Material: PLA Total area: Infill 4
Homogenous tumor model 2	Material: Nylon Total area: Infill 3	Material: Nylon Total area: Infill 1	Material: Nylon Total area: Infill 2
Heterogenous tumor model 1	Material: PLA Inner area: Infill 3 Outer area: Infill 7	Material: PETG Inner area: Infill 1 Outer area: Infill 5	Material: ASA Inner area: Infill 1 Outer area: Infill 2
Heterogenous tumor model 2	Material: PLA Inner area: Infill 2 Outer area: Infill 7	Material: PETG Inner area: Infill 1 Outer area: Infill 6	Material: ASA Inner area: Infill 1 Outer area: Infill 2

2.9. Breathing phantom for image registration studies

To obtain a ground-truth tumor motion we used ARDOS phantom [16]. The phantom has a removable rib cage and two lungs made from balsawood. Balsawood has the advantage of having low HUs as well as being a heterogeneous material with a HU distribution similar to lung tissue. Both the rib cage and the whole body including the lungs can be moved in axial direction to mimic breathing motion. Additionally, each lung has a borehole that enables to place inserts, which can be moved independently from the rest of the phantom. The inserts (Fig. 4b) are also made from balsawood and can hold tumors of different size. A holder cast from silicone (Fig. 4c) was constructed for reproducible positioning of the tumor phantoms inside the balsawood inserts (Fig. 4d, e). The materials used in ARDOS phantom are high density balsa wood, org. Photon/eSolid water and SB3 cortical bone for lung tissue, soft tissue in chest wall and bone tissues (ribs), respectively. The corresponding density (g/cm3), HU mean, and standard deviation for the three materials were 0.3, 1.04, 1.82 and -754 ± 32, 85 ± 10, 916 ± 42, respectively.

2.10. Measurements

3D CTs from the phantom were acquired at three positions of the tumor inserts simulating a breathing motion amplitude of 24 mm:

- position 1) the initial position simulating the maximum inspiration position,
- position 2) the tumor was moved forward 12 mm in longitudinal axis simulating a respiratory center position,
- position 3) the tumor moved another 12 mm forward in longitudinal axis simulating maximum expiration.

All CTs were acquired both with and without the rib cage placed inside ARDOS for every 3D printed tumor sample. Additionally, 2D projective X-ray images were acquired using the Elekta XVI imaging system in posterior-anterior (PA) and lateral (LAT) direction and again for every 3D printed tumor sample both with and without the rib cage placed inside ARDOS. The simulated breathing motion amplitude was again 24 mm but this time with steps of 2 mm leading to 13 imaging positions.

2.11. 3D/3D image registration

In order to perform the 3D/3D registration, we used the 3D Slicer toolbox using the General Registration (Elastix) module. In this study, for each tumor, the 3D registration was performed between CT images after two movements: 1) between images acquired at position 1 and position 2 (first motion), 2) between images acquired at position 2 and position 3 (second motion) (Section 2.10). The 3D/3D registration error

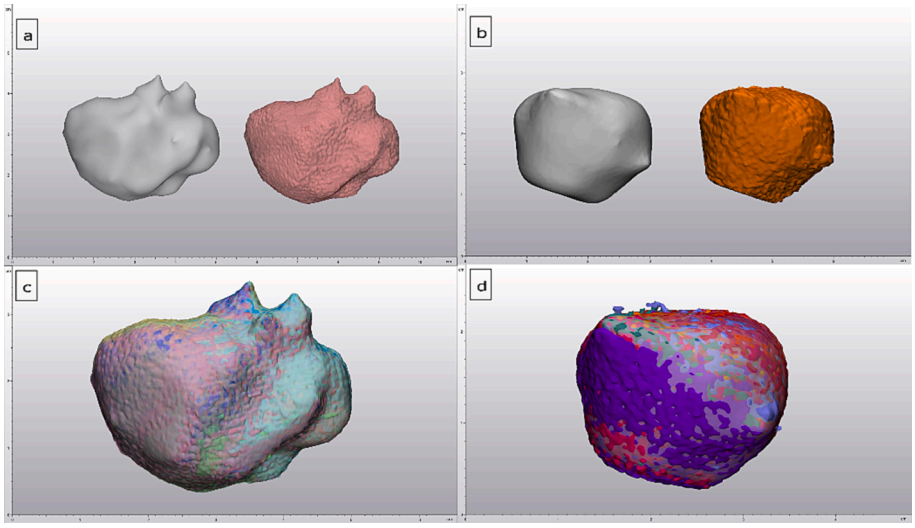

Fig. 3. Dimensional analysis workflow in 3-Matic 15.0 software. a) Digital models of patient (grey) and 3D printed tumor (pink) for tumor model 1, b) Digital models of patient (grey) and 3D printed tumor (orange) for tumor model 2, c) and d) Manual followed by automatic registration of six 3D printed tumor samples on the patient tumor models for tumor model 1 (c), tumor model 2 (d). The colors represent the different tumor sample models.

Table 2
Table showing the volume and surface area of the 3D printed tumor samples (samples 1–6 are related to both heterogenous and homogenous models), generated automatically in 3-Matic 15.0 software. This is directly based on the segmentation of the tumor CT images in Mimics Research 23.0. STD stands for standard deviation.

	Volume of tumor model 2 (mm3)	Surface area of tumor model 2 (mm2)
Patient	**5.344,81**	**1.882,12**
Sample 1	4.369,25	1.621,34
Sample 2	4.052,86	1.382,68
Sample 3	4.039,88	1.384,37
Sample 4	4.211,99	1.395,93
Sample 5	4.363,74	1.436,14
Sample 6	4.389,59	1.508,97
Mean ± STD over samples	4.237,89	1.454,90
	Volume of tumor model 1 (mm3)	**Surface area of tumor model 1 (mm2)**
Patient	**11.611,15**	**2.833,45**
Sample 1	11.480,50	2.997,60
Sample 2	11.477,12	2.978,05
Sample 3	11.551,95	2.954,48
Sample 4	11.633,25	3.328,17
Sample 5	11.402,31	3.154,86
Sample 6	11.666,98	3.056,08
Mean ± STD over samples	11.535,35	3.078,21

related to CC, LAT and PA directions as well as a 3D error by calculating the Root Mean Square Error (RMSE) over the errors from these three directions were calculated.

2.12. 2D/3D image registration

For 2D/3D registration the fast intensity-based image registration (FIRE) was used. FIRE is an in-house developed software for real time 2D/3D registration [25,26]. It uses digitally reconstructed radiographs (DRRs) generated from CT data which are registered to X-ray images. For the present study tumor registration was performed with an optimizer setting of 2 degrees of freedom (DoF). All 2D images (13 images with a motion step of 2 mm per measurement set) were registered to the CT in position 1) (Section 2.10).

3. Results

3.1. Resulting HU values for the printed cylinders

The four test cylinders with different infill density (Section 2.4) were printed successfully (Fig. 5 a). The CT scan from the four cylinders is presented in Fig. 5 b, c. A range between −217 to 226 HUs was achieved using four different materials (Table 3).

3.2. Additively manufactured tumor phantoms

All tumor phantoms from the two tumor models (Fig. 2 a, b) were successfully printed using the FDM printer. (Fig. 6).

3.3. Resulting radiodensity values for the tumor phantom

An axial slice from the patient and phantom CT are shown in Fig. 7. The printed heterogenous tumor sample 1 for model 1 showed an average radiodensity of 62 and −64 HU for inner and outer areas of the tumor (Table 4). In addition, the printed heterogenous tumor sample 1 for model 2 showed an average HU of 64 and −53 for inner and outer areas of the tumor. These results showed a good agreement between different radiodensity values of the proposed tumor phantom and the initial patient CT scan (average HUs of 0 to100 (=50 ± 34) HU for inner area and average HU of −100 to 0 (=-50 ± 29) for outer area) for the corresponding areas. The printed homogenous tumor sample 3 for model 1 and model 2 showed an average HU of 9 and −3 respectively. Additionally, these results showed a good match between the standard tumor phantom HU and the average patient tumor of −100 to 100 (=0) HU. The other tumor samples were designed to represent also other HU distribution ranges as observed in other patient tumor data (patient data which had some deviation from the average HU (-100 to 100)). The calculated density values (g/cm3) of all 3D printed phantoms are also presented in Table 5. As can be seen from the results of Table 5 and Table 1, the tumor phantoms with the infill densities that contained a higher percentage of air had lower density values, which was due to a lower weight.

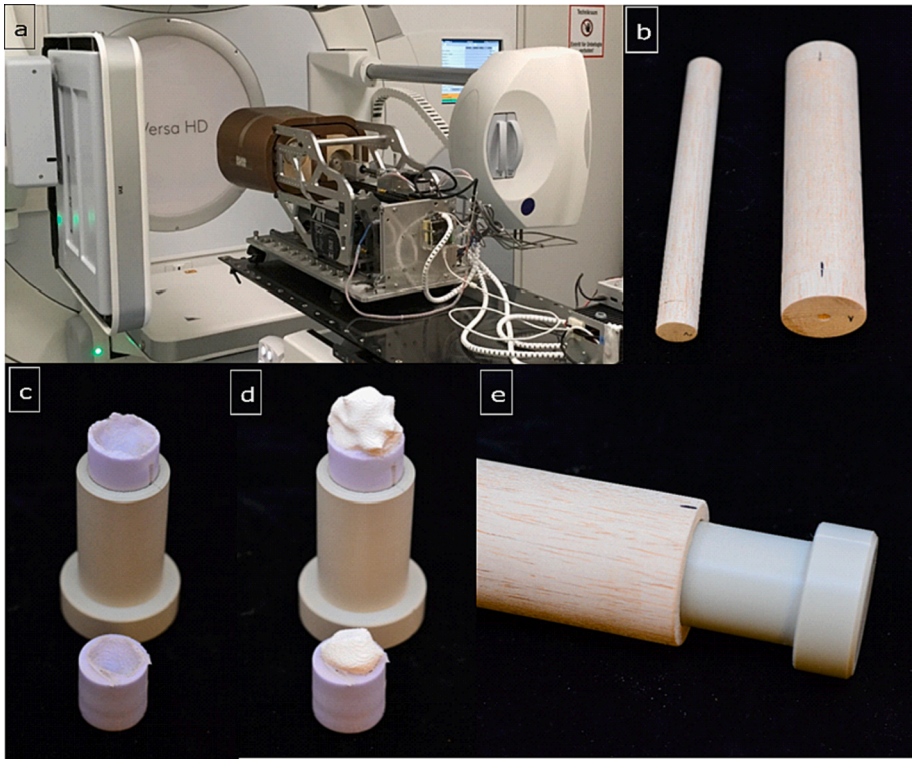

Fig. 4. The ARDOS breathing phantom (a) and the inserts which can hold printed tumors (b). A holder (c) was build for each of the tumor models with the exact imprint of the tumor to hold it in position (d) for reproduceible placement inside the insert (e).

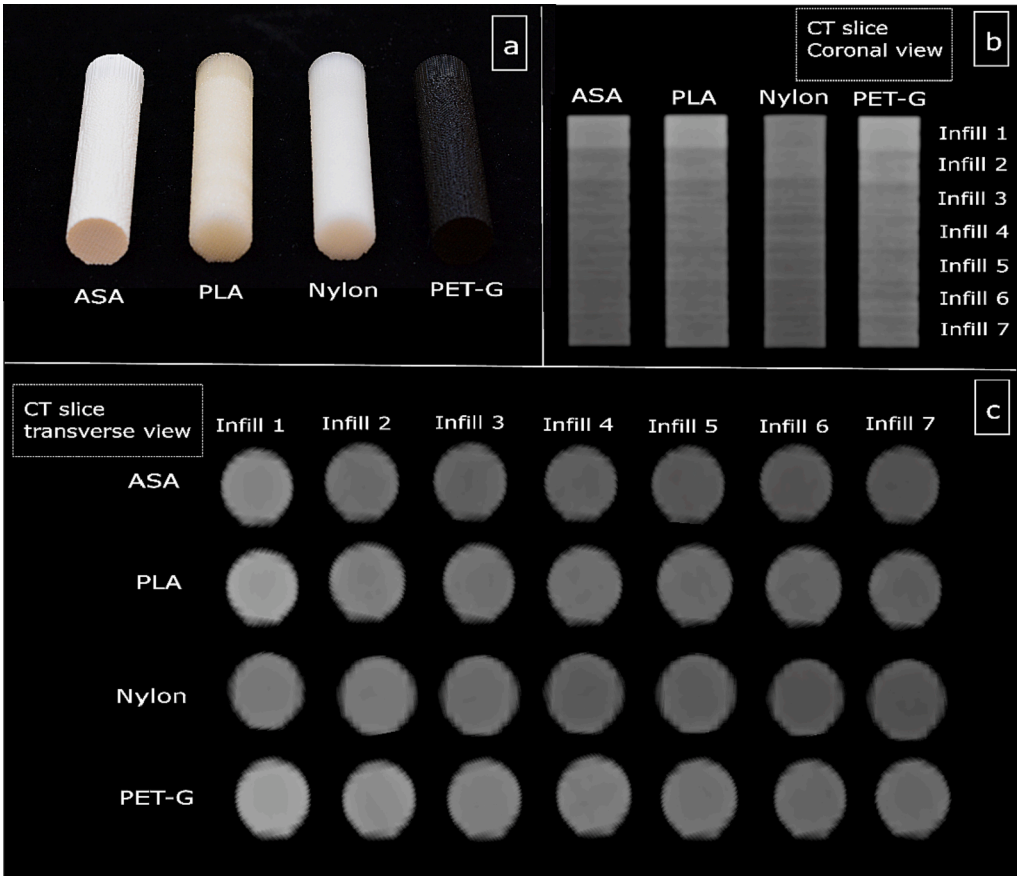

Fig. 5. (a) The printed cylinders with four different materials including ASA, PLA, Nylon and PETG. Coronal and transverse views of the CT image from four printed cylinders at different infill densities.

Table 3
HU values related to all cylinders from four different materials including ASA, PLA, Nylon and PETG at different infill densities. Std: standard deviation.

	Infill %	ASA (HU ± Std)	PLA (HU ± Std)	Nylon (HU ± Std)	PETG (HU ± Std)
Infill 1	100	155.30 ± 8	226.78 ± 14	50.14 ± 8	245 ± 8
Infill 2	97	19.13 ± 8	98.40 ± 10	18.43 ± 5	180.52 ± 14
Infill 3	94	−38.10 ± 8	65.72 ± 14	−56.12 ± 13	144.38 ± 16
Infill 4	91	−63.72 ± 17	7.23 ± 6	−93.36 ± 10	117.68 ± 14
Infill 5	88	−105.85 ± 13	−24.57 ± 8	−121.20 ± 13	85.39 ± 18
Infill 6	85	−130.79 ± 16	−47.85 ± 20	−185.34 ± 15	39.05 ± 13
Infill 7	82	−150.21 ± 14	−85.29 ± 11	−217.32 ± 14	−10.44 ± 7

3.4. 3D/3D registration results

According to the results, the average 3D RMSE over the three samples and different motions for the heterogenous tumor model 1 and tumor model 2 were 0.119 and 0.126, respectively. In addition, the average 3D RMSE over the three samples and the two motions for the homogenous tumor models1 and tumor model 2 were 0.102 and 0.108, respectively. These results show that for tumor model 1, the difference between 3D RMSE of heterogenous and homogenous design was 0.017. Furthermore, for tumor model 2, the difference between 3D RMSE of heterogenous and homogenous design was 0.018.

3.5. 2D/3D registration results

For PA imaging the 2D/3D registration was performed in CC/LAT directions. In addition, for LAT imaging the registration was done in CC/PA direction for both tumor models. The registration was successful on all X-ray images and total 2D errors of 0.043 mm and 0.035 mm was found for experiments without ribs for homogenous and heterogenous tumor samples, respectively (difference of 0.008 mm). In addition, total errors of 0.594 mm and 0.539 mm were found for the analysis including ribs for homogenous and heterogenous tumor samples, respectively (difference of 0.055 mm).

3.6. The results from the physical dimensional comparison between the phantom and patient STL

The results showed that the printed volume of the tumor, was lower respectively than that of the patient by 0.65 % for the tumor model 1 and 20.71 % for the tumor model 2 and the surface was rough with overall indentations; the surface area automatically generated by the 3-Matic 15.0 software was 8.64 % higher and 22.7 % lower than the patient model. During Collision Detection, the resulting volume overlap was 96.72 % for the tumor model 1 and 78.15 % for the tumor model 2 (Table 6).

3.7. Resulting HU values for the printed cylinders with continuous change of the HU

The CT scan from the two cylinders including 22 infills with step size 1 % is presented in Fig. 8. Ranges between −132 to 230 HUs and −65 to 256 HUs were achieved for PLA and PETG materials, respectively (Table 7). The CT result (Fig. 8) shows that a continuous change of the HU can be achieved when using step size of 1 %.

4. Discussion

In this study, a methodology for fabrication of CT-derived 3D printed tumor phantoms with realistic radiodensity and morphology were described. Four top materials qualified for mimicking the clinically relevant HU range for tumor tissues were introduced. Additionally, the infill densities of the materials were modulated in small step sizes to achieve a gray value spectrum equivalent to human lung tumor tissue (Table 2).

In this study, we proposed an FDM-based method for printing solid tumors with heterogeneous radiodensities. The different radiodensities as well as heterogeneous structures are achieved by differing the infill densities percentage. Application of different infill densities to create radiodensity heterogeneity in a single structure using 3D printing technology was introduced in our previous study [5] as well as in [27] for bony regions, but to our knowledge, it was the first time it was used for replication of realistic heterogeneity inside realistic 3d printed tumor imaging phantoms. Some previous studies focusing on the development of imaging tumor phantoms, reported limitations regarding replicating either the radiodensity or the structure compared to real patient tumor data [15,17]. In [15] CT-derived tumor phantoms using SLS technique were 3D printed and found to be geometrically highly accurate compared to real patient lung tumor data. However, the mean HU reported for fabricated two phantoms [15] was −478 HU and −130 HU which showed rather large differences with the corresponding reported tumor mean HU as in patients (-217 HU). In another study [17], although the proposed tumor phantoms radiodensity was in a good agreement with the patient tumor radiodensity, a realistic tumor shape and structure could not be reproduced using their approach based on injection of agar-gelatin. In addition, in a recent study the authors proposed direct 3D printing of the breast tumor phantoms using filament 3D printing technology [19]. However, the fabricated phantoms did not include realistic tumor radiodensity heterogeneity [19] and only a single

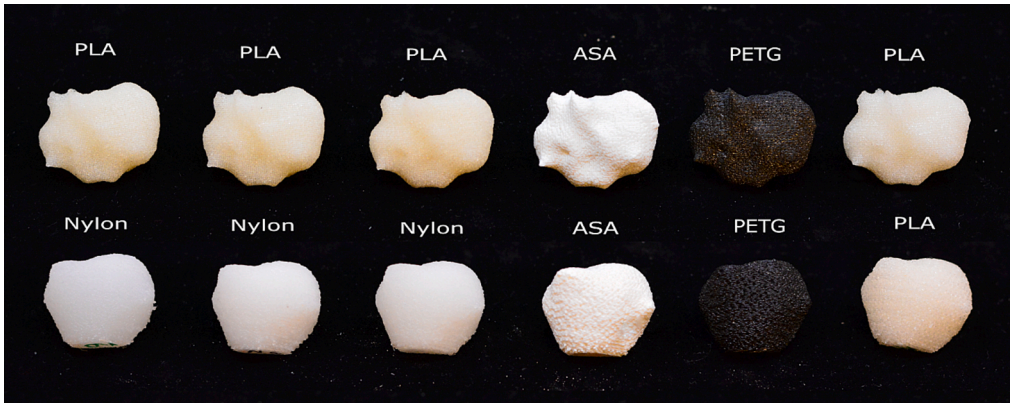

Fig. 6. The 3D printed tumor phantoms using four different materials including PLA, ASA, PETG and Nylon.

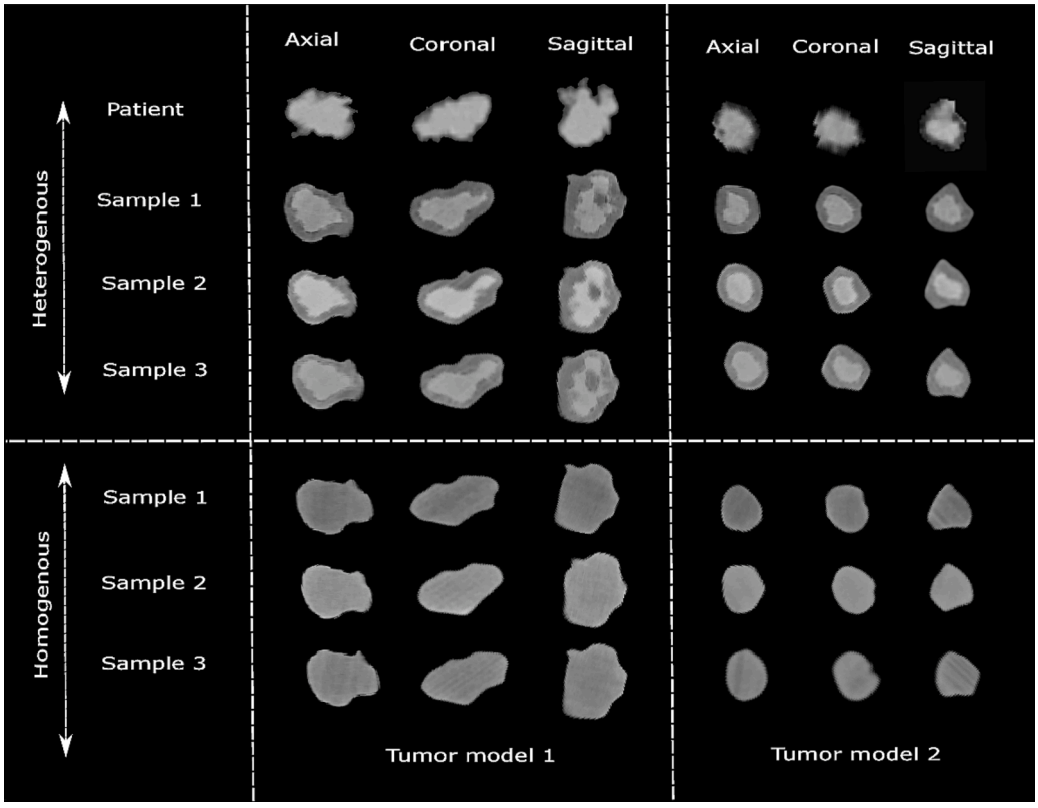

Fig. 7. An axial slice from the patient and tumor phantom CT for different tumor models and samples.

Table 4
HU values related to all printed tumor phantoms. Std: standard deviation.

	Sample 1 (HU ± Std)	Sample 2 (HU ± Std)	Sample 3 (HU ± Std)
Heterogenous tumor model 1	**Inner area** **Outer area** 62.43 ± 14–64.17 ± 9	**Inner area** **Outer area** 233.56 ± 7 78.86 ± 24	**Inner area** **Outer area** 138.12 ± 6 28.80 ± 9
Heterogenous tumor model 2	**Inner area** **Outer area** 64.64 ± 9–53.40 ± 18	**Inner area** **Outer area** 227.31 ± 10 46.83 ± 16	**Inner area** **Outer area** 152.18 ± 4 29.45 ± 6
Homogenous tumor model 1	**Total area** −74.80 ± 10	**Total area** 85.72 ± 12	**Total area** 9.53 ± 13
Homogenous tumor model 2	**Total area** −63.33 ± 7	**Total area** 53.94 ± 6	**Total area** −3.64 ± 25

Table 5
Density values (g/cm3) for all 12 tumor phantoms.

	Sample 1	Sample 2	Sample 3
Homogenous tumor model 1	Material: PLA density: 1.16 gcm^{-3}	Material: PLA density: 1.23 gcm^{-3}	Material: PLA density: 1.19 gcm^{-3}
Homogenous tumor model 2	Material: Nylon density: 1.11 gcm^{-3}	Material: Nylon density: 1.21 gcm^{-3}	Material: Nylon density: 1.17 gcm^{-3}
Heterogenous tumor model 1	Material: PLA density: 1.12 gcm^{-3}	Material: PETG density: 1.19 gcm^{-3}	Material: ASA density: 0.98 gcm^{-3}
Heterogenous tumor model 2	Material: PLA density: 1.13 gcm^{-3}	Material: PETG density: 1.18 gcm^{-3}	Material: ASA density: 1.03 gcm^{-3}

Table 6
Table showing the colliding volume between the 3D printed models (samples 1–6 are related to both heterogenous and homogenous models) and patient tumor model per sample, generated by Collision Detection function in 3-Matic 15.0 software. STD stands for standard deviation.

Model	Colliding volume of tumor model 1 (mm3)	Colliding volume of tumor model 2 (mm3)
Sample 1	11.291,33	4.243,47
Sample 2	11.076,82	4.048,21
Sample 3	11.245,25	4.034,05
Sample 4	11.299,77	4.179,00
Sample 5	11.115,99	4.305,23
Sample 6	11.355,22	4.251,84
Mean colliding volume	**11.230,73**	**4.176,97**
STD	**110,45**	**112,68**
% overlap	**96,72**	**78,15**
% failure	**−3,28**	**−21,85**

HU (64) was replicated inside the phantom. The only study which introduced direct fabrication of heterogeneity inside phantoms using different infill intensities within one single print with the goal of manufacturing realistic tumor phantoms was [18]; however, the printed phantom did not include realistic tumor shape and geometry and also only PET-G filament was examined in their experiments. Our proposed design enhances previous studies [15–19] by direct manufacturing of solid imaging tumor phantoms which can closely resemble patient tumor data regarding both geometry and radiodensity values and heterogeneity. In addition, we improve previous research by investigating appropriate filament materials, particularly for tumor phantom fabrication, by analyzing different filament density correspondence with realistic radiodensity range in patient tumor data. The large range of the resulting gray value spectrum with the corresponding infill density percentages reported in this study represents a lookup-table for researchers and phantom manufactures to create realistic CT tumor

Table 7
HU values related to the cylinders from two materials including PLA and PETG at different infill densities. Std: standard deviation.

	Infill %	PLA (HU ± Std)	PETG (HU ± Std)
Infill 1	100	230.78 ± 17	256 ± 10
Infill 2	99	130.12 ± 10	198.12 ± 18
Infill 3	98	118.61 ± 12	184.10 ± 15
Infill 4	97	112.32 ± 9	172.19 ± 12
Infill 5	96	100.12 ± 14	158.62 ± 16
Infill 6	95	98.24 ± 10	144.12 ± 9
Infill 7	94	86.16 ± 8	129.25 ± 12
Infill 8	93	74.12 ± 12	116.40 ± 10
Infill 9	92	61.9 ± 11	104.23 ± 8
Infill 10	91	50.18 ± 16	91.20 ± 10
Infill 11	90	38.9 ± 10	77.16 ± 15
Infill 12	89	22.14 ± 10	64.6 ± 12
Infill 13	88	8.11 ± 12	51.45 ± 10
Infill 14	87	−4.8 ± 9	37.12 ± 7
Infill 15	86	−18 ± 16	24.70 ± 12
Infill 16	85	−32.10 ± 14	11.10 ± 11
Infill 17	84	−45.8 ± 12	−4.24 ± 8
Infill 18	83	−60.9 ± 7	−17.23 ± 9
Infill 19	82	−79.12 ± 18	−29.12 ± 13
Infill 20	81	−97.8 ± 17	−40.35 ± 14
Infill 21	80	−115.6 ± 15	−52.70 ± 10
Infill 22	79	−132 ± 12	−65 ± 13

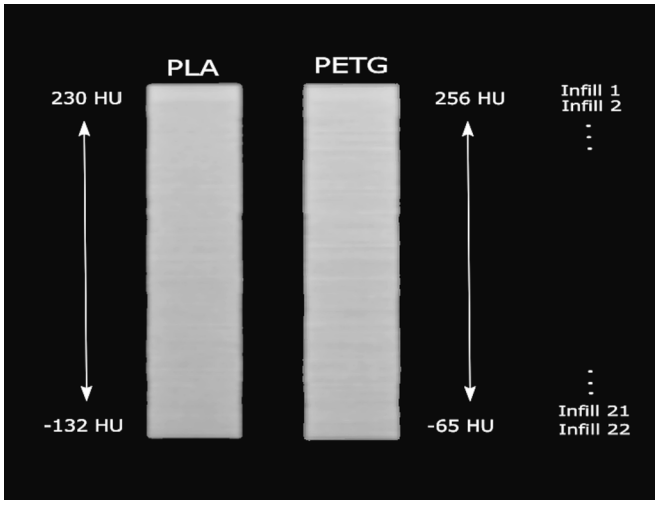

Fig. 8. (a) The printed cylinders with four different materials including PLA and PETG. Coronal views of the CT image from two printed cylinders (PLA and PETG) at different infill densities with step size of 1%.

phantoms at different body sites with the desired range of radiodensities.

This is the first study which proposes a phantom design that facilitates simulating complex radiodensity heterogeneity and geometry for tumor phantoms. In heterogenous tumor models, we selected only two infill densities, one for inner and one for outer volume which resulted to distinct HU difference. However, our experiments using some additional cylinder models also showed that a continuous change in HU can be achieved when using step size of 1 %. Therefore, tumor models that are more sophisticated with a gradient of HU can be designed by increasing the number of sub-volumes with different infill densities. Tumor phantoms separated from surrounding tissues, as proposed in this study, are beneficial for existing dynamic phantom (for example ARDOS breathing phantom which was used in this study or the commercially available CIRS Dynamic Thorax Phantom). They can be placed inside such phantoms and in this way the tumor phantom can be customized to replicate a realistic scenario.

A very low error difference (in the range of μm) was observed when comparing the 3D/3D and 2D/3D registration performance between homogenous and heterogenous tumor models. We assume the reason for this is the effect of projection imaging; the heterogeneity induces only small changes in the radiological properties because of the small tumor volume in comparison to large volume of the remaining tissue compartments along the projection of the torso. The results showed that homogenous tumors with realistic HU are sufficient for validation of 2D/3D registration algorithms. However, the heterogenous phantom design, as proposed in this study, can be used by other research groups to investigate whether such complexity would be required for an exact verification and validation of their algorithms. A possible example could be the verification of advanced image segmentation algorithms. Depending on the algorithm, sharp edges of an object play a vital role in the performance of segmentation. Here, simulating realistic HU distributions in the tumor phantom can be crucial when validating segmentation methods [28,29]. For performance evaluation of new imaging algorithms in the field of medical imaging, such as tumor tracking for tumor motion monitoring in RT or validation of advanced automatic segmentation methods for radiotherapy and interventional radiology, the fabricated tumor phantoms need to reproduce the radiological properties (mainly radiodensity) and tissue morphology as in the human body. Therefore, in terms of reproducing the radiodensity of the proposed phantoms, the main objective of this study was to achieve an HU value of the tumor tissue that is within the standard deviation of the actual HU value obtained from the patients' CT tumors (Section 2.1.1). In our experiments, we found a good agreement between the different radiodensity values of the proposed tumor phantom and the original CT scan of the patient (Section 3.3). Moreover, the geometry of such tumor phantoms should be as close as possible to human tumors. The results of Table 2 show that the volume and surface areas of the tumors phantoms agreed with the patient tumors.

Using the Collision Detection approach, the resulting volume overlap was 96.72 % for the tumor model 1 and 78.15 % for the tumor model 2. The observed error for the tumor model 2 can be attributed to the print resolution as the finer tumor geometry was not replicated in the smaller samples. Secondly, the threshold-based segmentation of the CT to generate digital models for comparison was pixelated, resulting in surface mismatch. In addition, the discrepancy observed for printed tumor volumes and the surface areas with respect to the real tumor volumes as observed in Table 2 originates from the smoothing step that was included when designing the tumor model from the real CT tumor (Section 2.2). Furthermore, the observed small differences in numbers between the degree of agreement in tumor model 1 and 2 between the patient and printed samples may arise due to the number of pixels included in the automatic contrast-based rendering process of the tumor and ultimately the dimensional calculation. The CT measurements performed in this study were limited to 120 kVp. Investigation of the radiological properties of the printed phantoms using other imaging settings including different energies, will also be part of our future work.

As another future perspective of this study, we will investigate some other modern 3D printers that offer the possibility to create heterogeneity in imaging phantoms. One potential 3D printing technique is multi-material extrusion 3D printing technology [30,31], which supports the combination of a large number of materials, including different silicone and filaments, in one 3D print and therefore may provide additional options for modulating radiological properties. In addition, in a previous study [32], we proposed macrostructure manipulation in STL design using Polyjet 3D printing technology, where a single material can mimic a range of radiation attenuations of human soft tissue. The possibility of using this approach to generate heterogeneity in tumor phantoms [32] will also be explored as a future point of this study.

5. Conclusion

This research investigated the construction, radiological properties and geometrical accuracy of additive manufacturing-based tumor

phantoms. This study lays the foundation of designing realistic and reliable tumor phantoms, which can be used for validation of different imaging algorithms in medical imaging area.

Declaration of Competing Interest

The authors declare that they have no known competing financial interests or personal relationships that could have appeared to influence the work reported in this paper.

Acknowledgment

This work has been supported by ACMIT – Austrian Center for Medical Innovation and Technology, which is funded within the scope of the COMET program and funded by Austrian BMVIT and BMWFW and the governments of Lower Austria and Tyrol.

References

[1] Kiarashi N, Nolte AC, Sturgeon GM, Segars WP, Ghate SV, Nolte LW, et al. Development of realistic physical breast phantoms matched to virtual breast phantoms based on human subject data. Med Phys 2015;42:4116–26. https://doi.org/10.1118/1.4919771.

[2] Hatamikia S, et al. Additively manufactured patient-specific anthropomorphic thorax phantom with realistic radiation attenuation properties. Front Bioeng Biotechnol 2020;8:385. https://doi.org/10.3389/fbioe.2020.00385.

[3] Mayer R, Liacouras P, Thomas A, Kang M, Lin L, Simone CB. 3D printer generated thorax phantom with mobile tumor for radiation dosimetry. Rev Sci Instrum 2015; 86:074301. https://doi.org/10.1063/1.4923294.

[4] Ehler ED, Barney BM, Higgins PD, Dusenbery E. Patient specific 3D printed phantom for IMRT quality assurance. Phys Med Biol 2014;59:5763–73. https://doi.org/10.1088/0031-9155/59/19/5763.

[5] Hatamikia S, Kronreif G, Unger A, Oberoi G, Jaksa L, Unger E, Koschitz S, Gulyas I, Irnstorfer N, Buschmann M, Kettenbach J, Birkfellner W, Lorenz A. 3D printed patient-specific thorax phantom with realistic heterogenous bone radiopacity using filament printer technology. Z Med Phys. 2022 Feb 24:S0939-3889(22)00007-1. doi: 10.1016/j.zemedi.2022.02.001. Epub ahead of print. PMID: 35221154.

[6] Buytaert D, Taeymans Y, De Wolf D, Bacher K. Evaluation of a no-reference image quality metric for projection X-ray imaging using a 3D printed patient-specific phantom. Phys Med 2021 Sep;89:29–40. https://doi.org/10.1016/j.ejmp.2021.07.011. Epub 2021 Jul 31 PMID: 34343764.

[7] Deene Y, Wheatley M, Greig T, Hayes D, Ryder W, Loh H. A multi-modality medical imaging head and neck phantom: Part 1. Design and fabrication. Phys Med 2022 Apr;96:166–78. https://doi.org/10.1016/j.ejmp.2022.02.010. Epub 2022 Feb 19 PMID: 35190265.

[8] Filippou V, Tsoumpas C. Recent advances on the development of phantoms using 3D printing for imaging with CT, MRI, PET, SPECT, and ultrasound. Med Phys 2018;45:740–60. https://doi.org/10.1002/mp.13058.

[9] Homolka P, Figl M, Wartak A, Glanzer M, Dünkelmeyer M, Hojreh A, et al. Design of a head phantom produced on a 3D rapid prototyping printer and comparison with a RANDO and 3 M lucite head phantom in eye dosimetry applications. Phys Med Biol 2017;62:3158–74. https://doi.org/10.1088/1361-6560/aa602c.

[10] Niebuhr NI, Johnen W, Güldaglar T, Runz A, Echner G, Mann P, et al. Technical note: Radiological properties of tissue surrogates used in a multimodality deformable pelvic phantom for mr-guided radiotherapy. Med Phys 2016;43(43): 908–16. https://doi.org/10.1118/1.4939874.

[11] Tino R, Yeo A, Leary M, Brandt M, Kron T. A systematic review on 3D-printed imaging and dosimetry phantoms in radiation therapy Technol. Cancer Res Treat 2019;18. https://doi.org/10.1177/1533033819870208.

[12] Bliznakova K, Dukov N, Feradov F, Gospodinova G, Bliznakov Z, Russo P, et al. Development of breast lesions models database. Phys Med 2019 Aug;64:293–303. https://doi.org/10.1016/j.ejmp.2019.07.017. Epub 2019 Aug 3 PMID: 31387779.

[13] Dukov N, Bliznakova K, Feradov F, Buliev I, Bosmans H, Mettivier G, et al. Models of breast lesions based on three-dimensional X-ray breast images. Phys Med 2019 Jan;57:80–7. https://doi.org/10.1016/j.ejmp.2018.12.012. Epub 2018 Dec 27 PMID: 30738536.

[14] Okkalidis N. 3D printing methods for radiological anthropomorphic phantoms. Phys Med Biol. 2022 Jul 27;67(15). doi: 10.1088/1361-6560/ac80e7. PMID: 35830787.

[15] Hazelaar C, van Eijnatten M, Dahele M, Wolff J, Forouzanfar T, Slotman B, et al. Using 3D printing techniques to create an anthropomorphic thorax phantom for medical imaging purposes. Med Phys 2018;45:92–100. https://doi.org/10.1002/mp.12644.

[16] Kostiukhina N, Georg D, Rollet S, Kuess P, Sipaj A, Andrzejewski P, et al. Advanced Radiation DOSimetry phantom (ARDOS): a versatile breathing phantom for 4D radiation therapy and medical imaging. Phys Med Biol 2017;62:8136–53. https://doi.org/10.1088/1361-6560/aa86ea.

[17] Sramek M, Shi Y, Quintanilla E, Wu X, Ponukumati A, et al. Tumor phantom for training and research in transoral surgery. Lary Inves Otolary 2020;16:677–82. https://doi.org/10.1002/lio2.426.

[18] Rinaldi L, Pezzotta F, Santaniello T, De Marco P, Bianchini L, Origgi D, et al. HeLLePhant: A phantom mimicking non-small cell lung cancer for texture analysis in CT images. Phys Med 2022 May;97:13–24. https://doi.org/10.1016/j.ejmp.2022.03.010. Epub 2022 Mar 22 PMID: 35334407.

[19] Dukov N, Bliznakova K, Okkalidis N, Teneva T, Encheva E, Bliznakov Z. Thermoplastic 3D printing technology using a single filament for producing realistic patient-derived breast models. Phys Med Biol. 2022 Feb 10;67(4). doi: 10.1088/1361-6560/ac4c30. PMID: 35038693.

[20] Varallo A, Sarno A, Castriconi R, Mazzilli A, Loria A, Del Vecchio A, et al. Fabrication of 3D printed patient-derived anthropomorphic breast phantoms for mammography and digital breast tomosynthesis: Imaging assessment with clinical X-ray spectra. Phys Med 2022 Jun;98:88–97. https://doi.org/10.1016/j.ejmp.2022.04.006. Epub 2022 May 5 PMID: 35526373.

[21] Dancewicz OL, et al. Radiological properties of 3D printed materials in kilovoltage and megavoltage photon beams. Phys Medica 2017;38:111–8. https://doi.org/10.1016/j.ejmp.2017.05.051.

[22] Solc J, et al. Tissue-equivalence of 3D-printed plastics for medical phantoms in radiology. J Instruct 2018;13. https://doi.org/10.1088/1748-0221/13/09/P09018.

[23] Ivanov D, Bliznakova K, Buliev I, Popov P, Mettivier G, Russo P, et al. Suitability of low density materials for 3D printing of physical breast phantoms. Phys Med Biol 2018 Sep 6;63(17):175020. https://doi.org/10.1088/1361-6560/aad315. PMID: 29999497.

[24] https://www.jiga.io/calculator/density/asa/gml.

[25] Furtado H, Steiner E, Stock M, Georg D, Birkfellner W. Real-time 2D/3D registration using kV-MV image pairs for tumor motion tracking in image guided radiotherapy. Acta Oncol 2013;52:1464–71. https://doi.org/10.3109/0284186x.2013.814152.

[26] Wolfgang Birkfellner1, Michael Figl, Hugo Furtado, Andreas Renner, Sepideh Hatamikia and Johann Hummel, Multi-Modality Imaging: A Software Fusion and Image-Guided Therapy Perspective. Front Phys 2018; 6: 66. https://doi.org/10.3389/fphy.2018.00066.

[27] Ma X, Figl M, Unger E, Buschmann M, Homolka P. X-ray attenuation of bone, soft and adipose tissue in CT from 70 to 140 kV and comparison with 3D printable additive manufacturing materials. Sci Rep 2022 Aug 26;12(1):14580. https://doi.org/10.1038/s41598-022-18741-4. PMID: 36028638; PMCID: PMC9418162.

[28] C. Militello, L. Rundo, M. Dimaco, A. Orlando,R. Woitek, et al., 3D DCE-MRI Radiomic Analysis for Malignant Lesion Prediction in Breast Cancer Patients. Acad Radio 2021 (in press). https://doi.org/10.1016/j.acra.2021.08.024.

[29] N. Sharma, L.M. Aggarwal Automated medical image segmentation techniques. J Med Phys 2010; 35: 3-14. 10.4103/0971-6203.58777.

[30] JAKSA, Laszlo et al. Development of a Multi-Material 3D Printer for Functional Anatomic Models. International Journal of Bioprinting, [S.l.], v. 7, n. 4, p. 420, oct. 2021. ISSN 2424-8002.

[31] Jaksa L, Pahr D, Kronreif G, Lorenz A. Development of a Multi-Material 3D Printer for Functional Anatomic Models. Int J Bioprint 2021 Oct 12;7(4):420. https://doi.org/10.18063/ijb.v7i4.420. PMID: 34805598; PMCID: PMC8600298.

[32] Hatamikia S, Oberoi G, Zacher A, Kronreif G, Birkfellner W, Kettenbach J, Ponti S, Lorenz A, Buschmann M, Jaksa L, Irnstorfer N, Unger E. Additively manufactured test phantoms for mimicking soft tissue radiation attenuation in CBCT using Polyjet technology. Z Med Phys. 2022 Jul 2:S0939-3889(22)00063-0. doi: 10.1016/j.zemedi.2022.05.002. Epub ahead of print. PMID: 35792011.